Infrared Spectroscopy of Matrix Isolated Polycyclic Aromatic Hydrocarbons. 1. PAHs Containing Two to Four Rings

Douglas M. Hudgins* and Scott A. Sandford

National Aeronautics and Space Administration Ames Research Center, MS 245-6, Moffett Field, California 94035

Received: April 25, 1997[⊗]

Matrix isolation techniques have been used to measure the mid-infrared spectra of the polycyclic aromatic hydrocarbons (PAHs) naphthalene, anthracene, phenanthrene, 1,2-benzanthracene, chrysene, pyrene, tetracene, and triphenylene. The band positions and relative strengths are compared to previous laboratory studies, where available, and with available theoretical calculations.[1] Comparisons with theory indicate that density functional theory (DFT) does an excellent job of describing the majority of the infrared active fundamentals of the PAHs considered here. Band positions typically match to within 5 cm^{-1}, with the worst mismatches usually no more than 15 cm^{-1}. Matches in band strengths are not as precise but, with the exception of the CH stretching bands, are generally good to better than 35% for most strong and moderate bands and to factors of 2 to 3 for weaker bands. Theory predicts CH stretching band strengths that are about a factor of 2 times too strong. The laboratory spectra contain large numbers of bands due to overtone/combination modes that are not considered in the calculations, and while most of these bands are weak, some can be moderately strong. Finally, comparisons between the infrared spectra of matrix isolated PAHs and a common family of interstellar emission bands confirm that neutral PAHs do not provide a good fit to the astronomical data. Neutral PAHs produce features having appropriate frequencies but generally inappropriate strengths. Nevertheless, significant contributions from PAH neutrals may be required to explain the spectra of a few less energetic astronomical environments.

I. Introduction

Polycyclic aromatic hydrocarbons, or simply PAHs, represent one of the most stable families of organic compounds known. Their stability is afforded by π-electron delocalization within the sp^2-hybridized benzenoid moieties of their structures and leads to the family's ubiquity in the terrestrial environment. They are the dominant component of coals and coal-derived liquids and an important byproduct of petroleum manufacture.[2] They are a major component of the soot formed in virtually all combustion processes[3] and, as such, represent important environmental pollutants. Their importance as pollutants stems from their well-documented biological activity.[4]

In addition to their terrestrial importance, extensive observational and experimental work over the past decade has indicated that PAHs are the dominant class of molecular species in the interstellar medium (ISM). PAH molecules, in one form or another, have been proposed as the carriers of an ubiquitous family of interstellar infrared emission features near 3050 cm^{-1} (3.3 μm), 1920 cm^{-1} (5.2 μm), 1610 cm^{-1} (6.2 μm), 1310 cm^{-1} (7.7 μm), 1160 cm^{-1} (8.6 μm), 885 cm^{-1} (11.3 μm), 840 cm^{-1} (11.9 μm), and 787 cm^{-1} (12.7 μm) seen in the spectra of reflection nebulae, planetary nebulae, and regions containing ionized hydrogen gas.[5−7] The variety of objects and conditions under which these emission features are seen suggests that PAHs are common throughout the ISM, and their intensity indicates that they represent the most abundant interstellar polyatomic molecules known, perhaps accounting for as much as 10% of all the carbon in the galaxy.[6]

The interstellar PAH theory was founded on the general resemblance of the interstellar emission spectra to the laboratory absorption spectra of aromatic hydrocarbons. The earliest laboratory absorption work was largely restricted to the simplest PAH, naphthalene ($C_{10}H_8$), in solution and in crystals.[8] This work was later augmented by the excellent and comprehensive theoretical and experimental work of Cyvin and co-workers.[9] All of this work dealt with neutral PAHs in condensed phases (pure crystals, KBr salt pellets, and organic solvents). Some more recent work on PAHs in KBr salt pellets has also been done to examine the temperature dependence of PAH infrared absorption.[10] In the condensed phase, interactions of the PAHs with the surrounding medium and with other PAH molecules (clusters) can strongly alter the frequencies and intensities of the vibrational modes.[7] As a result, while this body of spectroscopic information has proven invaluable in establishing the interstellar PAH theory, further progress has been hindered by the lack of spectroscopic data on PAHs under conditions more relevant to the astrophysical problem.

Observational studies by Sellgren[11] confirmed that the interstellar infrared emission is nonthermal in nature. It is produced by the radiative "cooling" of PAHs excited by the absorption of single UV or visible photons. This implies that the interstellar PAHs exist as free molecules in the gas-phase rather than in solid clusters or grains where thermalization of absorbed energy is faster than infrared emission at fundamental frequencies. Thus, to properly address the astrophysical problem, spectroscopic data for PAHs which are free from the perturbations of intermolecular interactions are needed. Over the last several years an impressive array of both theoretical

* To whom correspondence should be addressed.

[⊗] Abstract published in *Advance ACS Abstracts,* December 15, 1997.

S1089-5639(98)03481-1 CCC: $15.00
Published on Web 01/08/1998

and experimental effort has been brought to bear on this problem. Extensive theoretical calculations of the vibrational frequencies and intensities for a number of neutral PAHs have been carried out by several groups.[1,12,13] Laboratory work satisfying this constraint fall into two broad categories: (1) gas-phase studies and (2) matrix isolation studies.

A number of reports of the vibrational spectroscopy of gas-phase PAHs have appeared in the literature over the past several years. Absorption spectra of gas-phase PAHs generated by thermal vaporization have been reported, including a variety of PAHs in the 2−4 ring size range, as well as a few larger PAHs and some polycyclic aromatic compounds containing side groups or heteroatoms.[14−16] In addition, elegant UV-pumped infrared emission experiments on gas-phase PAHs have begun to address the very difficult task of experimentally measuring the emission spectra of these molecules.[17−19] Together, the results of these experiments show that (i) the peak emission frequency of the aromatic CH stretch in gas-phase PAHs shifts to lower frequencies with increased internal energy content and is consistent with that of the interstellar 3050 cm^{-1} band at reasonable levels of excitation, (ii) the bandwidth increases with energy and matches that of the interstellar 3050 cm^{-1} band at similarly appropriate internal energies, and (iii) a broad emission plateau underlying this feature and extending out to about 2740 cm^{-1}, a feature which is observed in a number of astronomical objects, is reproduced as well.

While such research is extremely important in establishing and exploring the implications of the PAH theory and to understanding the molecular physics of the emission process, this work is hampered by (i) the thermalization of the gas-phase PAH molecules in the experiment and (ii) the difficulty in measuring the lower frequency vibrational modes of these molecules. In the interstellar medium, electronic excitation of the PAHs occurs through the absorption of single UV and visible photons. These electronically excited molecules are quickly converted to high vibrational levels of the ground electronic state through a rapid isoenergetic internal conversion process.[6] Nevertheless, while this process leads to the formation of *vibrationally* hot molecules ($T_{vib} \approx 1000$ K), angular momentum conservation in these isolated molecules prevents distribution of the molecular energy among its rotational modes. As a result, the interstellar molecules remain *rotationally* cool ($T_{rot} \approx 100$ K). Thus, there is also a need for reliable quantitative infrared spectral data on individual PAHs at the low temperatures characteristic of the interstellar medium. The matrix isolation technique is well suited to this task.

In matrix isolation a species of interest is isolated in a solid, rare-gas matrix at low temperatures for study. Since interactions with the inert matrix material are weak, the molecules are trapped in a quasi-gas-phase environment. In this matrix environment the temperature is low (≈10 K), molecular rotations are hindered, and the low rotational excitation of PAHs in the ISM is approximated. The positions of the absorption bands of most matrix isolated molecules typically undergo only small shifts in the 0−15 cm^{-1} range relative to their gas-phase values[20] and this has been shown to be true of PAHs as well.[15,16] Only a limited number of PAHs have been studied in matrix isolation.[21−30]

To expand this database and to address the astrophysical infrared emission problem, we have undertaken a systematic survey of the mid-infrared spectra of a large number of PAHs. This work has been carried out in conjunction with similar studies of the spectroscopy of ionized PAHs.[22−25] This paper reports the mid-infrared spectra of the smallest PAHs: those containing from two to four benzenoid rings. The adjoining articles in this series which follow in this journal volume focus on, respectively, the mid-infrared spectra of larger neutral PAHs containing five or more benzenoid rings (part 2)[31] and the mid-infrared spectra of a series of PAHs which incorporate a cyclopentadienyl ring in their structures (part 3).[32] Additional recent spectroscopic studies of matrix isolated perdeuterated PAHs and PAHs containing a variety of chemical sidegroups can be found elsewhere.[13,33]

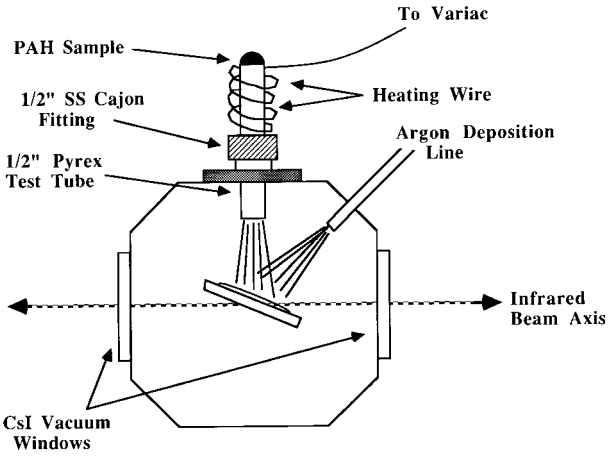

Figure 1. Schematic of the sample chamber used in these experiments.[22,23] The chamber is approximately 10 cm across. The UV lamp was not used in these experiments.

This paper is organized as follows. Details of the experimental procedure employed are discussed in section II. In section III, the spectra of the neutral PAHs are presented and compared to available theoretical data (section III.B) and their implications for astrophysics are discussed (section III.C). Finally, the key results are summarized in section IV.

II. Experimental Section

The matrix isolation technique was employed to isolate individual polycyclic aromatic hydrocarbon (PAH) molecules in an argon matrix where their infrared spectra were measured. The experimental apparatus and methodology have been described in detail previously[13,22−24] and will be reviewed only briefly here.

A schematic cross-section of the sample chamber is shown in Figure 1. An infrared transparent window (CsI) is suspended inside a high-vacuum chamber ($P \approx 10^{-8}$ Torr) and cooled by a closed-cycle Helium refrigerator. The vacuum chamber is equipped with multiple inlet ports, and the cooler is mounted so that the infrared window can be rotated to face any of the ports without breaking vacuum. Initially, the CsI window is cooled to 10 K and positioned to face a sample deposition inlet. Samples were prepared by co-deposition of a gaseous PAH with a large overabundance of argon until an appropriate thickness is produced.

The smallest PAH, naphthalene, is sufficiently volatile that it was possible to premix it in the gas phase in a sample bulb with a known amount of argon at room temperature. The data presented here were obtained from an Ar/naphthalene mixture of 1200/1. PAHs containing more than two rings require thermal vaporization of a solid sample with simultaneous co-deposition of larger amounts of argon. To this end, all the other PAH samples were deposited from resistively heated Pyrex tubes mounted on the sample chamber. Sample temperatures were monitored using a chromel/alumel-type K thermocouple mounted

on the exterior of the tube. During PAH volatilization, argon was admitted through an adjacent inlet port in such a way that the two "streams" coalesced and froze together on the surface of the cold window. The argon deposition line was liquid nitrogen trapped to minimize contamination.

The PAHs used in this investigation were naphthalene ($C_{10}H_8$, Aldrich, 99+% purity), anthracene ($C_{14}H_{10}$, Aldrich, 95% purity), phenanthrene ($C_{14}H_{10}$, Aldrich, 98+% purity), pyrene ($C_{16}H_{10}$, Aldrich, 99% purity), 1,2-benzanthracene ($C_{18}H_{12}$, Aldrich, 99% purity), chrysene ($C_{18}H_{12}$, Aldrich, 98% purity), tetracene ($C_{18}H_{12}$, Aldrich, nominal 98% purity), and triphenylene ($C_{18}H_{12}$, Aldrich, nominal 98% purity). Significant impurities were detected in the samples of tetracene and triphenylene. These impurities had a somewhat higher volatility than the associated PAHs and were, thus, largely removed by vacuum bake-out near their sublimation temperatures for a period of several hours prior to deposition. Otherwise, samples were used without further purification. Matheson prepurified argon (99.998% min.) was used as the matrix material.

Sample quality was found to be optimal for PAH deposition vapor pressures in the range from 10 to 30 mTorr. Higher vapor pressures necessitated high Ar flow rates, which exceeded the thermal conductivity of the CsI window, warmed the matrix and resulted in "annealing", which increased scattering toward higher frequencies. Conversely, lower vapor pressures require longer deposition times, thereby increasing background contamination (primarily H_2O) in the matrix. Optimum deposition temperatures for the PAHs discussed here were anthracene, 35 °C; phenanthrene, 13 °C (cooled); pyrene, 65 °C; 1,2-benzanthracene, 85 °C; chrysene, 95 °C; tetracene, 125 °C; and triphenylene, 85 °C. The optimal argon flow rate was estimated to be between 0.5 and 1.0 mmol/h. On the basis of this flow rate and the PAH deposition rates calculated from integrated band areas and using the theoretical intrinsic band strengths, the argon/PAH ratios in all samples were found to be well in excess of 1000/1.

After sample deposition was complete, spectral measurements were executed by rotating the cold head to face the beam of an infrared spectrometer. The sample chamber was equipped with CsI vacuum windows and suspended in the sample compartment of an FTIR spectrometer. Mid-infrared spectra (7000−500 cm^{-1}) were collected using an MCT-B detector/KBr beam splitter combination. All spectra reported here were measured at a resolution of 0.9 cm^{-1} (the width of an unresolved line) using a data-sampling spacing of 0.23 cm^{-1}. Spectra were typically generated through coaddition of 5 blocks of 200 scans, a number which optimized both the signal-to-noise ratio and time requirements of each experiment.

Band strengths were integrated from absorbance spectra using an algorithm provided with the spectrometer. Such integrations depend on the choice of baseline for each band. Comparisons between integrations made with different choices of reasonable baselines demonstrated that the choice of base line results in variations of total band strength that are typically less than 5%, but may be as high as 50% for the weakest features.

III. Results and Discussion

A. Conventions Used in the Figures and Tables. Matrix isolation infrared spectra and tabular summaries of the measured band positions and relative strengths are presented in the following sections. These positions and strengths are then compared to available theoretical calculations.[1] The following conventions used in the presentation of the data.

1. Absorption Bands Due to Contaminant H_2O. While the PAHs are responsible for the vast majority of the absorption bands seen in all the spectra, the matrices also contain low levels of background H_2O. The dominant features of matrix isolated H_2O fall in the 1625−1590 cm^{-1} range, with the strongest bands near 1624, 1608, and 1593 cm^{-1}. When clearly visible, these bands are marked with a solid dot (•) in the figures that follow.

2. Site Effects and Band Splitting. It is not uncommon for the absorption features produced by matrix isolated species to be split or to display substructure. Such substructure commonly arises from species trapped in different matrix sites, each seeing slightly different molecular environments. This "site-splitting" is small, typically no more than 10 cm^{-1}. On the other hand, matrix perturbations can also split bands simply by lifting vibrational degeneracies. In practice it can be difficult to determine whether multiple, closely spaced absorption bands are due to matrix effects or to distinctly different vibrational modes that happen to have similar frequencies. Therefore, multiple bands are specially noted in the tabulations. In those cases where one of the bands dominates in strength, its position is listed with a footnote indicating that it is the strongest member of a band "complex". In those cases where there is no obvious dominant feature, or where there is reason to believe the bands may be associated with different vibration modes, each of the band positions are specified.

3. Comparison to Theoretical Predictions. In the tables, the experimental band positions and relative intensities are compared with the recent, comprehensive calculations of Langhoff.[1] That work employed density functional theory (DFT) to determine the harmonic frequencies and intensities of all the neutrals discussed in this paper. The tables contain positions and relative intensities for all bands down to a threshold intensity of 1% that of the strongest band in the 900−600 cm^{-1} aromatic CH out-of-plane bending region. In those cases where an experimental or theoretical relative band strength exceeds the 0.01 threshold, but the corresponding to theoretical/experimental value does not, both are included. In some cases this necessitated the addition of theoretical bands that did not appear in the original publication. Those bands are noted with a "†" in the tables.

In addition, the experimental spectra of matrix isolated PAHs contain a significant number of bands that are not predicted by the theoretical models. While it is possible that in some cases these mismatches between theory and experiment represent a failure of the model calculations, the vast majority of these bands are probably due to overtone/combinations of lower frequency modes and to site effects. The theory predicts only bands due to fundamental vibrations and therefore does not address such features. Some discrepancies may also be due to infrared *inactive* modes that are weakly induced by matrix interactions.

4. Low-Frequency Limits. The previous theoretical studies included vibrational modes as low as 90 cm^{-1}. However, in its current configuration, the system used for our laboratory measurements is only capable of operating down to about 450 cm^{-1}. As a result, the experimental data do not address bands below this frequency. Nevertheless, the theoretical values have been included in the tables for completeness. For the low-frequency emission spectra of several PAHs, see Zhang et al.[34]

5. The CH Stretching Region, 3150−2900 cm^{-1}. Comparisons between the experimental and theoretical data in the 3150−2900 cm^{-1} spectral region are particularly problematic. While this region is dominated by aromatic CH stretching vibrations, additional features arising from overtone/combinations of lower frequency modes are also observed. Some of these features

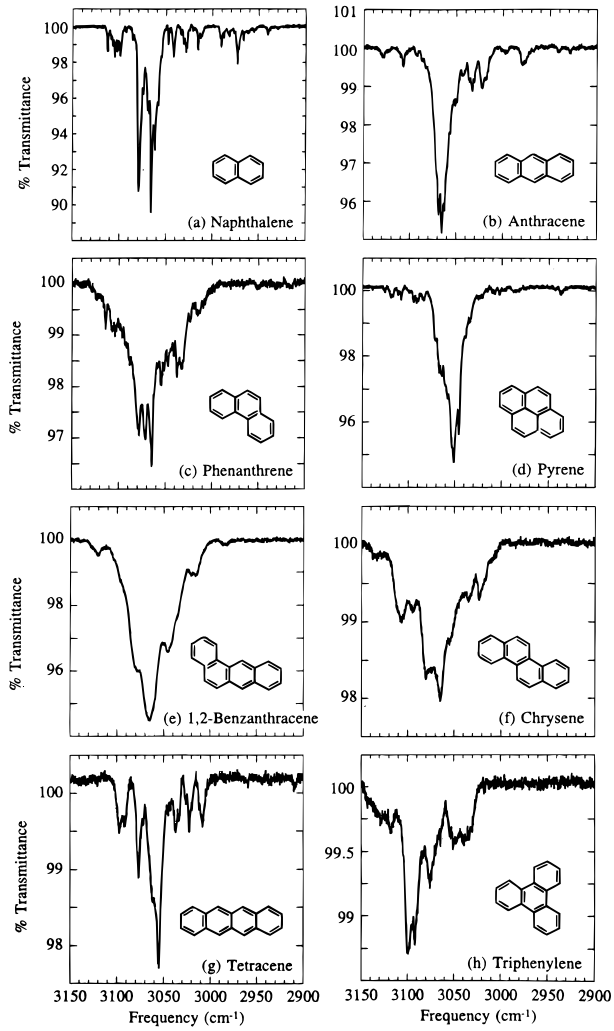

Figure 2. Spectra in the 3150−2900 cm^{-1} CH stretching region of the matrix isolated PAHs: (a) naphthalene ($C_{10}H_8$), (b) anthracene ($C_{14}H_{10}$), (c) phenanthrene ($C_{14}H_{10}$), (d) pyrene ($C_{16}H_{10}$), (e) 1,2-benzanthracene ($C_{18}H_{12}$), (f) chrysene ($C_{18}H_{12}$), (g) tetracene ($C_{18}H_{12}$), and (h) triphenylene ($C_{18}H_{12}$). All matrixes were deposited and measured at 10 K. The argon to PAH ratio was 1200/1 for naphthalene and well in excess of 1000/1 for the other PAHs.

can be quite strong if they are in Fermi resonance with one of the fundamental CH stretching vibrations. As a result, the CH stretching region in the experimental spectra is always more complex than predicted by theory. Furthermore, the experimental bands in this region overlap extensively, precluding the measurement of individual strengths. Therefore, in the tables, while the *positions* of all significant features seen in the 3150−2900 cm^{-1} region are listed with the strongest bands indicated as such, only the *total* integrated absorption over the *entire* region spanned by the bands is listed. This total absorption is then be compared with the *sum* of all the predicted bands in this region.

B. The Infrared Spectra of Neutral Matrix isolated PAHs. In the sections that follow, the 3150−2900 cm^{-1} and 2000−500 cm^{-1} infrared spectra of naphthalene ($C_{10}H_8$), anthracene ($C_{14}H_{10}$), phenanthrene ($C_{14}H_{10}$), pyrene ($C_{16}H_{10}$), 1,2-benzanthracene, chrysene, tetracene, and triphenylene (all $C_{18}H_{12}$) are presented. The strengths and positions of the bands in these spectra are then compared to theoretical predictions and previous experimental work where available. The characteristic aromatic CH stretching region will be considered first for all the PAHs *en masse*, followed by discussions of the 2000−500 cm^{-1} data for each PAH individually.

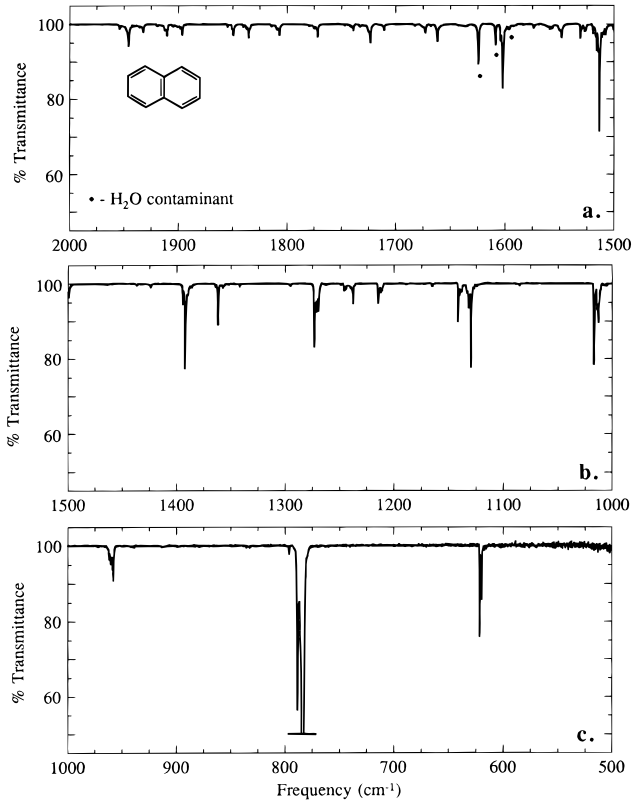

Figure 3. The spectra of matrix isolated naphthalene ($C_{10}H_8$) through the aromatic CC stretching and CH bending regions: (a) 2000−1500 cm^{-1}, (b) 1500−1000 cm^{-1}, and (c) 1000−500 cm^{-1}. The strongest CH out-of-plane bending mode band has been truncated to enhance visibility of features across the spectrum. The sample was deposited and measured at 10 K and the argon-to-naphthalene ratio was 1200/1.

1. The CH Stretching Region, 3150−2900 cm^{-1}. The 3150−2900 cm^{-1} matrix isolation spectra of all eight PAHs can be found in Figure 2a−h. The positions of the strongest experimental bands agree well with those predicted by theory (see Tables 1−8, vide infra). The other features are most likely overtones and combinations of lower frequency modes.

While the theory provides decent matches in position, relative band strengths are more problematic. Specifically, comparisons between the data sets reveal that the theoretical calculations consistently overestimate the absorption intensity in this region by the following factors: naphthalene, factor of 2.2; anthracene, 1.7; phenanthrene, 1.8; pyrene, 1.9; 1,2-benzanthracene, 2.4; chrysene, 2.2; tetracene, 2.4; and triphenylene, 2.5. These, in fact, represent a *lower* limit to the mismatches since some of the measured absorption in this region is certainly due to the aforementioned, unrelated overtone/combination bands. Although some portion of these discrepancies may be due to matrix effects since gas-phase frequencies and intensities of the PAHs pyrene, coronene, and ovalene are observed to fall somewhat closer to the theoretical predictions,[15,35] most are due to limitations in the theoretical treatment.[36] The experimental measurements confirm the results of extensive calibration calculations which indicated that the relatively small 4-31G basis set used for the theoretical calculations yields CH stretching intensities that are high by about a factor of 2. Thus, it would appear qualitatively that the measured relative intensities reported here are accurate.

2. Naphthalene, $C_{10}H_8$. The 2000−500 cm^{-1} spectrum of matrix isolated naphthalene is presented in Figure 3. The positions and strengths of the absorption bands are listed and

TABLE 1: Infrared Frequencies (cm^{-1}) and Intensities for Neutral Naphthalene

experiment		theory[a]			
frequency in Ar (cm^{-1})	relative intensity[b]	irreducible representation	frequency (cm^{-1})	intensity (km/mol)	relative intensity[c]
d		b_{3u}	171.8	1.9	0.02
d		b_{1u}	360.6	1.3	0.01
473.7	0.17	b_{3u}	480.0	16.0	0.14
621.2, 619.3	0.04	b_{2u}	632.1	3.2	0.03
783.4, 788.2	1.00	b_{3u}	788.4	111.3	1.00
957.6[e]	0.03	b_{3u}	963.5	4.3	0.04
1016.4, 1012.4	0.07	b_{2u}	1009.7	4.1	0.04
1129.1[e]	0.05	b_{1u}	1131.9	3.2	0.03
1140.9[e]	0.02				
1164.3, 1164.8	0.002	b_{2u}	1169.7	1.2	0.01
1214.2[e]	0.02	b_{2u}	1208.8	1.2	0.01
1237.1[e]	0.02				
1272.8[e]	0.07	b_{1u}	1270.0	8.2	0.07
1361.6	0.02	b_{2u}	1358.3	1.5	0.01
1391.8[e]	0.06	b_{1u}	1399.8	3.2	0.03
1498.9	0.01				
1513.0[e]	0.06	b_{2u}	1507.9	9.1	0.08
1604.4	0.06	b_{1u}	1593.3	6.3	0.06
1722.4	0.02				
1945.1	0.02				
2939.8					
2965.7					
2972.2					
2981.6					
2989.7					
3014.9					
3027.7					
3041.1		b_{1u}	3043.5	8.7	0.08
3046.8		b_{2u}	3045.4	1.4	0.01
3061.2					
3065.0[f]		b_{1u}	3062.5	78.7	0.71
3078.2[f]		b_{2u}	3076.5	71.3	0.64
3098.2					
3101.3					
3104.1					
3106.2					
3111.7					
Σ 3117-2934	0.65				
sum =				160.1	1.44

[a] Taken from ref 1. [b] Intensities relative to that of the combined 783.4 and 788.2 cm^{-1} bands. [c] Theoretical intensities given relative to the strength of the calculated 788.4 cm^{-1} band. [d] Theoretical position lying below the low-frequency limit of experimental data. [e] Position of strongest band or bands in a "complex" of features. [f] Major feature in the CH stretching region.

TABLE 2: Infrared Frequencies (cm^{-1}) and Intensities for Neutral Anthracene

experiment		theory[a]			
frequency in Ar (cm^{-1})	relative intensity[b]	irreducible representation	frequency (cm^{-1})	intensity (km/mol)	relative intensity[c]
d		b_{3u}	91.0	1.0	0.01
d		b_{1u}	232.3	1.3	0.02
468.0[e]	0.20	b_{3u}	471.3	17.3	0.23
602.9	0.09	b_{2u}	612.7	7.5	0.10
725.6, 729.6[e]	1.00	b_{3u}	730.2	76.4	1.00
878.3	0.77	b_{3u}	885.3	63.9	0.84
906.8, 908.5	0.01	b_{1u}	908.0	1.7	0.02
954.9[e]	0.07	b_{3u}	962.0	8.6	0.11
1000.9	0.08	b_{2u}	1000.7	3.2	0.04
1149.2	0.07	b_{1u}	1156.2	4.7	0.06
		b_{2u}	1157.7	3.4	0.04
1166.9	0.05	b_{2u}	1169.3	1.0	0.01
1272.5	0.06	b_{1u}	1274.6	10.2	0.13
1318.1	0.10	b_{1u}	1311.2	2.0	0.03
1345.6, 1346.4	0.02	b_{2u}	1342.6	4.2	0.05
1450.5	0.04	b_{2u}	1455.3	3.6	0.05
1460.0	0.03	b_{1u}	1456.1	2.1	0.03
1542.0[e]	0.08	b_{2u}	1533.7	5.0	0.06
1610.5	0.02	b_{1u}	1620.0	7.9	0.10
1627.8	0.04				
1675, 1683.5	0.03				
1707.2[e]	0.04				
1738.3	0.02				
1765.4	0.04				
1780.0[e]	0.01				
1796.7[e]	0.05				
1815.8[e]	0.03				
1844.1	0.01				
1903.8[e]	0.02				
1918.3, 1924.5	0.03				
1938.1[e]	0.06				
2979.1					
3021.6		b_{1u}	3039.0	10.7	0.14
3032.0		b_{1u}	3044.1	18.7	0.24
3064.6[f]		b_{1u}	3063.2	81.3	1.06
		b_{2u}	3077.8	95.5	1.25
3106.4					
3127.9					
Σ 3136-2918	1.63				
sum =				206.2	2.69

[a] Taken from ref 1. [b] Intensities relative to that of the combined absorbance produced by the complex that contains the 725.6 and 729.6 cm^{-1} bands. [c] Theoretical intensities given relative to the strength of the calculated 730.2 cm^{-1} band. [d] Theoretical position lying below the low-frequency limit of experimental data. [e] Position of strongest band in a "complex" of features. [f] Major feature in the CH stretching region.

compared to their theoretically predicted values[1] in Table 1. The relative strengths of the bands were normalized to the strong band pair at 783.4 and 788.2 cm^{-1} in the experimental data and to the predicted band at 788.4 cm^{-1}.

In general, the agreement between experiment and theory is remarkable. The average difference in the frequencies of predicted and observed bands is only about 5 cm^{-1}, and all the differences are less than 11 cm^{-1}. Relative band strengths also compare favorably, although there is greater variation. The relative strengths of the stronger bands generally agree to within 25%. The only moderate band that shows disagreement at the factor-of-2 level falls at 1391.8 cm^{-1}. Experimentally, the intensity is measured to be about twice that predicted by theory (theory, 0.03; experiment, 0.06). Weaker bands agree to within better than a factor of 2.

While these results provide a more complete listing of bands to greater sensitivity, they are entirely consistent with earlier matrix isolation studies of naphthalene[22,26] (see Table 2 in ref 1). The agreement in band positions, even to the level of satellite bands due to matrix effects, is excellent; differences rarely exceed the level of reported precision. While there is some variation between reported relative strengths for the CH stretching features, this is likely due to differences in the baselines and frequency ranges used for the band integrations.

3. Anthracene, $C_{14}H_{10}$. The 2000−500 cm^{-1} spectrum of matrix isolated anthracene is presented in Figure 4. The positions and strengths of the absorption bands are listed in Table 2 together with their theoretically calculated values.[1] The relative strengths of the bands were normalized to the sum of the band complex dominated by the 725.6 and 729.6 cm^{-1} features in the experimental data and to the predicted band at 730.2 cm^{-1}.

Again, the agreement between experiment and theory is excellent. The average difference in the frequencies of predicted and observed bands in Table 2 is again on the order of 5 cm^{-1}, and all are less than 10 cm^{-1}. Relative band strengths also compare favorably, although not as well as in the case of naphthalene. The relative strengths of most strong bands agree to within about 50% or better. Weaker bands agree to within better than factors of 2−4.

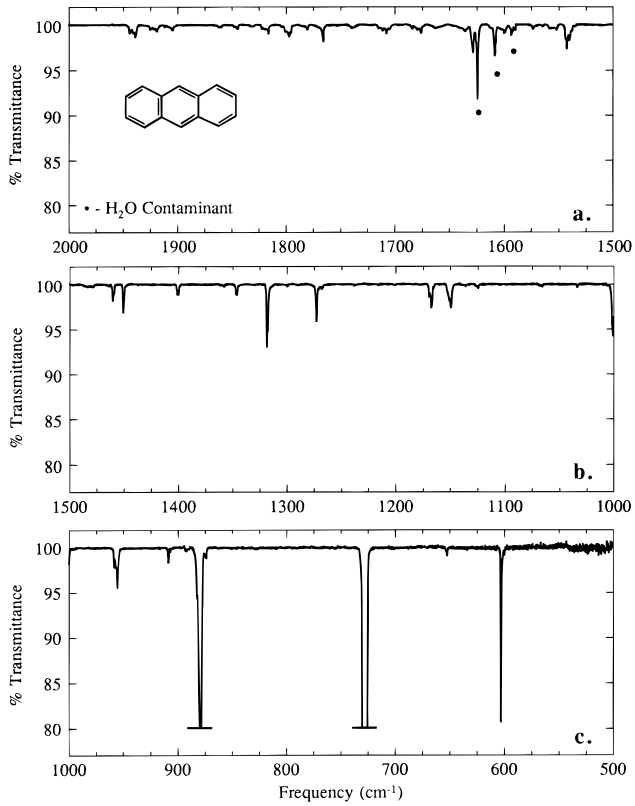

Figure 4. The spectra of matrix isolated anthracene ($C_{14}H_{10}$) through the aromatic CC stretching and CH bending regions: (a) 2000−1500 cm^{-1}, (b) 1500−1000 cm^{-1}, and (c) 1000−500 cm^{-1}. Several of the strongest CH out-of-plane bending mode bands have been truncated to enhance visibility of features across the spectrum. The sample was deposited and measured at 10 K and the argon-to-anthracene ratio was in excess of 1000/1.

Although the differences are not dramatic, a number of bands of moderate intensity do differ from their predicted strengths by somewhat larger factors than was typical for naphthalene. These include the bands at 1000.9 cm^{-1} (experiment ∼2 times stronger than theory), 1272.5 cm^{-1} (experiment ∼2 times weaker than theory), 1318.1 cm^{-1} (experiment ∼3 times stronger than theory), and the 1345.6−1346.4 cm^{-1} doublet (experiment ∼2 times weaker than theory). There are band strength differences associated with several other bands as well. For instance, the experimentally observed 1149.2 and 1166.9 cm^{-1} bands (relative intensities 0.07 and 0.05, respectively) differ both in the number of bands observed and in the distribution of their absorption from the predicted 1156.2, 1157.7, and 1169.3 cm^{-1} bands (0.06, 0.04, and 0.01, respectively). Nevertheless, the *total* absorption in this region matches well. Finally, while contaminant H_2O hinders quantitative comparisons in the 1630−1590 cm^{-1} region, bands are observed at 1610.5 and 1627.8 cm^{-1} that may correspond to the predicted 1620.0 cm^{-1} feature.

As with naphthalene, these results, while more comprehensive, are in good agreement with the earlier matrix isolation studies of anthracene[28] (see Table 3 in ref 1). The agreement in both band positions and intensities is excellent. The data sets only differ significantly in the 1630−1590 cm^{-1} region where H_2O contamination leads to greater uncertainty in the experimental measurements.

4. Phenanthrene, $C_{14}H_{10}$. The 2000−500 cm^{-1} spectrum of matrix isolated phenanthrene is presented in Figure 5. The positions and strengths of the absorption bands are listed and compared to theoretical predictions[1] in Table 3. The relative strengths of the bands were normalized to the sum of the band

TABLE 3: Infrared Frequencies (cm^{-1}) and Intensities for Neutral Phenanthrene

experiment		theory[a]			
frequency in Ar (cm^{-1})	relative intensity[b]	irreducible representation	frequency (cm^{-1})	intensity (km/mol)	relative intensity[c]
d		b_1	226.8†	2.9	0.04
d		b_1	430.5	5.6	0.07
d		b_2	440.0†	1.7	0.02
494.0	0.04	b_1	498.4	3.9	0.05
		b_2	500.1†	0.8	0.01
617.5, 618.8	0.06	b_2	627.8	4.6	0.06
710.2, 714.5	0.04	b_1	715.1†	1.5	0.02
		b_2	716.7†	2.4	0.03
735.0[e]	1.00	b_1	736.6	74.6	1.00
812.8[e]	0.69	b_1	817.0	59.7	0.80
833.0	0.02				
864.9[e]	0.12	b_2	870.2†	1.4	0.02
877.6	0.02	b_1	871.4	11.1	0.15
948.2[e]	0.03	b_1	950.3	4.2	0.06
1002.5, 1003.7	0.02	b_2	999.0†	1.4	0.02
1039.9, 1044.3	0.06	b_2	1038.3	3.6	0.05
1094.5, 1095.9	0.02	a_1	1093.0†	0.9	0.01
1144.1	0.03	b_2	1148.3†	1.3	0.02
1165.4	0.02				
1202.7	0.03	a_1	1203.0†	2.0	0.03
1223.8	0.006	b_2	1224.6†	0.9	0.01
1245.8, 1250.6	0.11	a_1	1250.3	9.4	0.13
1302.9	0.04	a_1	1298.8†	1.6	0.02
1351.4	0.01	a_1	1343.4†	2.2	0.03
1419.0	0.01	a_1	1417.8†	1.0	0.01
1427.5	0.01				
1430.7	0.02				
1436.2	0.007				
1447.9	0.005	a_1	1443.9	3.6	0.05
1460.4	0.14	b_2	1461.7	14.3	0.19
1504.7, 1505.9	0.09	b_2	1497.3	7.1	0.10
1530.1, 1531.8	0.02	a_1	1521.6†	1.8	0.02
1597.9	0.01	a_1	1595.1	4.5	0.06
1602.8	0.004	a_1	1610.5†	0.8	0.01
1946.7[e]	0.04				
2951.0					
3013.7					
3031.1					
3036.9					
3046.4		a_1	3045.1	5.5	0.07
		b_2	3045.8†	2.9	0.04
3053.9		a_1	3057.0	18.3	0.24
3063.6[f]		a_1	3063.6	47.1	0.63
3070.9[f]		b_2	3070.7	52.8	0.71
		a_1	3075.2†	2.7	0.04
3078.2[f]		b_2	3082.5	36.3	0.49
3106.0		a_1	3093.3	32.9	0.44
3113.1					
Σ 3119-3006 sum =	1.47			198.5	2.66

[a] Taken from ref 1. † indicates theoretical band not reported in original publication. [b] Intensities relative to the combined absorbance of produced by the complex dominated by the 735.0 cm^{-1} band. [c] Theoretical intensities given relative to the strength of the calculated 736.6 cm^{-1} band. [d] Theoretical position lying below the low-frequency limit of experimental data. [e] Position of strongest band or bands in a "complex" of features. [f] Major feature in the CH stretching region.

complex dominated by the 735.0 cm^{-1} feature in the experimental data and to the predicted band at 736.6 cm^{-1}.

Again, the agreement between experiment and theory is superb. The average difference in the frequencies of predicted and observed bands is 4 cm^{-1} with all differences less than 9 cm^{-1}. Relative band strengths also compare favorably, with those of both the moderate and strong bands agreeing to within 30% and the weaker bands to within better than a factor of 2.

Only a few bands require any additional comment. First, theory predicts a weak band near 1417.8 cm^{-1} (0.01) and a moderately weak feature near 1443.9 cm^{-1} (0.05) that are

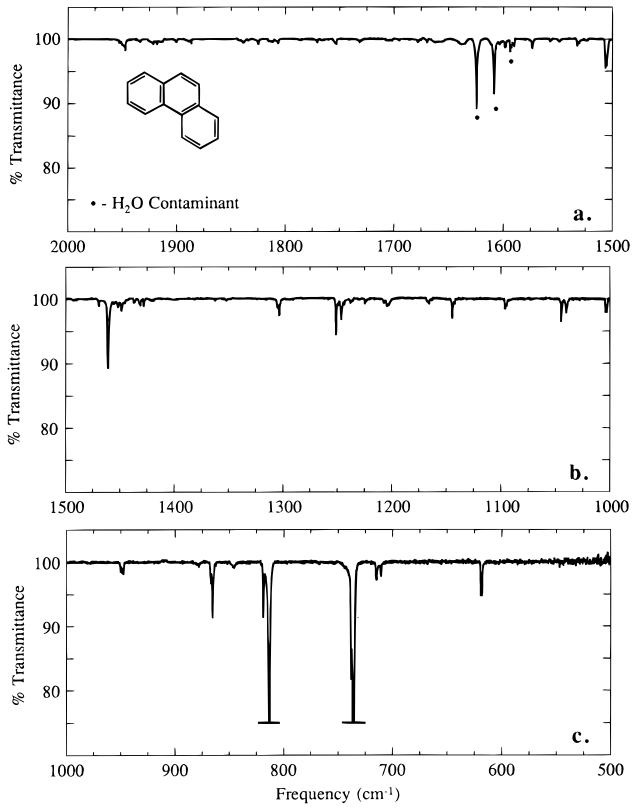

Figure 5. The spectra of matrix isolated phenanthrene ($C_{14}H_{10}$) through the aromatic CC stretching and CH bending regions: (a) 2000−1500 cm^{-1}, (b) 1500−1000 cm^{-1}, and (c) 1000−500 cm^{-1}. Several of the strongest CH out-of-plane bending mode bands have been truncated to enhance visibility of features across the spectrum. The sample was deposited and measured at 10 K and the argon-to-phenanthrene ratio was in excess of 1000/1.

difficult to uniquely assign to the experimentally observed bands at 1419.0 (0.01), 1427.5 (0.01), 1430.7 (0.02), 1436.2 (0.007), and 1447.9 cm^{-1} (0.005). Nonetheless, the *combined* strengths of these bands match fairly well between theory and experiment. Second, theory predicts a feature having similar strength at 1595.1 cm^{-1} (0.06). A feature is observed at 1597.9 cm^{-1}, but it is approximately 6 times weaker (0.01). This discrepancy is likely due to interference with contaminant H_2O in the experimental spectrum, however. Finally, while their individual strengths could not be integrated separately, the combined intensity of the experimental 710.2 and 714.5 cm^{-1} (0.04) features agrees well with the sum of the predicted bands at 715.1 and 716.7 cm^{-1} (0.05).

Previous work on matrix isolated phenanthrene has not been reported. However, comparisons can be made with the unpublished gas-phase work of Joblin (private communication and Table 6 in ref 1). The agreement in band positions is generally very good, although the gas-phase values generally fall 6−8 cm^{-1} to lower frequencies relative to the matrix values. Presumably, this is due to the temperature difference between the matrix (10 K) and the gas-phase experiments (673 K). Recent studies have shown that the IR bands of PAHs shift toward lower frequencies with increasing temperature.[16] A shift of 6 to 8 cm^{-1} is entirely reasonable given the temperature difference between the matrix and gas-phase experiments. There are also several theoretically predicted bands (1497.3, 1443.9, and 950.3 cm^{-1}) detected in the matrix spectra but not reported in the gas phase.

The discrepancies in band strengths between the gas-phase experiments and theory are largely similar to those observed

TABLE 4: Infrared Frequencies (cm^{-1}) and Intensities for Neutral Pyrene

experiment		theory[a]			
frequency in Ar (cm^{-1})	relative intensity[b]	irreducible representation	frequency (cm^{-1})	intensity (km/mol)	relative intensity[c]
d		b_{3u}	210.0	7.3	0.06
d		b_{2u}	353.5	1.4	0.01
487.6	0.01	b_{3u}	491.2	1.5	0.01
499.2	0.01	b_{1u}	499.6	2.5	0.02
542.6	0.02	b_{2u}	549.2	2.5	0.02
711.8, 715.0	0.43	b_{3u}	710.9	32.0	0.27
743.9[e]	0.17	b_{3u}	746.6	9.9	0.08
821.5	0.05	b_{1u}	819.7	3.1	0.03
842.8[e]	1.00	b_{3u}	848.3	120.5	1.00
964.1	0.01	b_{3u}	976.8	2.4	0.02
1097.3	0.04	b_{1u}	1092.3	4.8	0.04
1164.5	<0.01	b_{2u}	1160.8	1.7	0.01
1183.9[e]	0.19	b_{2u}	1188.3	10.3	0.09
1243.0[e]	0.04	b_{1u}	1253.1	3.6	0.03
1312.1[e]	0.03	b_{2u}	1314.6	6.5	0.05
1434.8[e]	0.12	b_{1u}	1427.0	11.8	0.10
		b_{2u}	1427.5†	1.2	0.01
1471.0	0.02	b_{2u}	1476.2	4.0	0.03
1581.3	0.005	b_{1u}	1586.1	12.8	0.11
1604.0	0.08	b_{2u}	1597.0	5.5	0.05
1792.6[e]	0.07				
1911.5	0.01				
1918.0	0.02				
1930.6	0.05				
2937.5					
2987.3					
3002.7					
3007.7					
3023.6					
3044.6		b_{1u}	3041.6†	3.6	0.03
		b_{2u}	3053.5	23.2	0.19
3050.2[f]		b_{2u}	3063.2	94.7	0.79
3064.8		b_{1u}	3073.8	95.8	0.79
3083.9					
3090.0					
3091.8					
3094.8					
3108.4					
3111.8					
3118.5					
3125.7					
Σ 3128-3026 sum =	0.97			217.3	1.80

[a] Taken from ref 1. † indicates theoretical band not reported in original publication. [b] Intensities relative that of the combined absorbance produced by the complex whose strongest band lies at 842.8 cm^{-1}. [c] Theoretical intensities given relative to the strength of the calculated 848.3 cm^{-1} band. [d] Theoretical position lying below the low-frequency limit of experimental data. [e] Position of strongest band in a "complex" of features. [f] Major feature in the CH stretching region.

for the matrix isolation data with the exception of the predicted 1595.1 cm^{-1} band, the theoretical strength of which is in considerably better agreement with the gas-phase data which is free from H_2O contamination. Finally, there is no evidence of a band in the matrix isolation data which might correspond to the gas-phase band reported at 998 cm^{-1}. The theoretical calculations do not predict a band at this location.

5. Pyrene, $C_{16}H_{10}$. The 2000−500 cm^{-1} spectrum of matrix isolated pyrene is presented in Figure 6. The positions and strengths of the absorption bands are listed and compared to theoretical predictions[1] in Table 4. The relative strengths of the bands were normalized to the sum of the band complex dominated by the 842.8 cm^{-1} feature in the experimental data and to the predicted band at 848.3 cm^{-1}.

Pyrene has a high degree of symmetry for a tetracyclic PAH (D_{2h}), and thus it possesses a relatively small number of infrared active modes. Consequently, the agreement between experiment

TABLE 5: Infrared Frequencies (cm^{-1}) and Intensities for Neutral 1,2-Benzanthracene

experiment		theory[a]			
frequency in Ar (cm^{-1})	relative intensity[b]	irreducible representation	frequency (cm^{-1})	intensity (km/mol)	relative intensity[c]
d		a″	183.6†	0.8	0.01
d		a″	266.7†	0.7	0.01
d		a′	301.6†	0.7	0.01
d		a″	422.2†	2.7	0.04
d		a′	448.8†	1.9	0.03
467.8	0.14	a″	468.6	9.5	0.14
508.5	0.03	a″	513.1†	1.0	0.02
539.0	0.07	a″	539.5	4.6	0.07
565.2	0.03	a″	570.5†	1.7	0.03
576.4	0.07	a′	580.9	4.3	0.06
621.0	0.03	a′	631.4†	2.4	0.04
650.0	0.05	a′¥	656.0	3.7	0.06
685.3	0.06	a″	688.3	3.9	0.06
737.4	0.04	a″	739.7†	2.1	0.03
747.0	1.00	a″	748.9	67.2	1.00
758.5	0.02	a′	758.5†	1.2	0.02
782.5	0.07	a″	779.2	10.7	0.16
804.9	0.28	a″	808.5	20.8	0.31
876.0 } 882.5[e]	0.67	a′	871.0†	2.9	0.04
		a″	882.9	54.9	0.82
908.4	0.003	a″	903.6	6.7	0.10
943.9	0.02	a″	943.2	3.3	0.05
951.7	0.05	a″	956.4	5.4	0.08
985.8	0.02	a′	980.3†	0.1	0.001
1010.3	0.03	a′	1008.2†	1.8	0.03
1040.3	0.05	a′	1038.1	3.2	0.05
1133.7	0.02	a′	1134.7†	1.5	0.02
1141.9	0.01	a′	1157.2†	1.7	0.03
1155.4	0.03	a′	1167.8†	1.5	0.02
1173.9	0.03	a′	1184.0†	2.8	0.04
1216.9	0.01	a′	1204.2†	0.9	0.01
1222.9[e]	0.03	a′	1223.6†	2.3	0.03
1240.2	0.07	a′	1242.7	7.6	0.11
1276.3 } 1280.7 }	0.08	a′	1266.4†	1.0	0.01
		a′	1289.3†	2.6	0.04
1299.5, 1309.5[e]	0.13	a′	1299.4†	1.1	0.02
1326.5	0.02	a′	1317.0†	1.0	0.02
1340.9	0.03	a′	1338.9	4.3	0.06
1359.1[e]	0.03	a′	1352.9†	2.3	0.03
1411.4, 1416.6	0.02	a′	1415.7†	1.2	0.02
1432.8	0.02	a′	1418.6†	0.9	0.01
1459.0	0.05	a′	1457.4	5.9	0.09
1478.0, 1483.4	0.05	a′	1479.5	3.6	0.05
1504.6	0.18	a′	1495.7	18.8	0.28
1552.1	0.02	a′	1540.5†	2.2	0.03
1607.8	0.01	a′	1598.8†	1.2	0.02
1615.6	0.01	a′	1611.7†	1.2	0.02
1623.6	0.01	a′	1618.1	3.0	0.04
1678.9	0.06				
1748.7	0.02				
1762.1	0.01				
1768.7	0.01				
1808.3[e]	0.04				
1835.0, 1839.3	0.02				
1902.8	0.01				
1917.8	0.05				
1944.9[e]	0.07				
2983.1					
3016.5		a′	3039.6	4.7	0.07
		a′	3042.8†	1.6	0.02
3044.5		a′	3043.7	11.8	0.18
		a′	3045.9	3.4	0.07
		a′	3047.7†	1.8	0.03
		a′¥	3055.8	9.6	0.14
		a′	3063.0	8.3	0.12
3064.1[f]		a′	3064.0	61.5	0.92
		a′	3064.8	22.1	0.33
		a′	3075.1	38.0	0.57
3077.6		a′	3078.9	54.1	0.81
3119.5		a′	3089.0	27.8	0.41
Σ 3131-2977	1.54				
sum =				244.7	3.67

[a] Taken from ref 1. † indicates theoretical band not reported in original publication. ¥ symmetry incorrectly listed as a" in original publication. [b] Intensities relative to the strongest observed band at 747.0 cm^{-1}. [c] Theoretical intensities given relative to the strength of the calculated 748.9 cm^{-1} band. [d] Theoretical position lying below the low-frequency limit of experimental data. [e] Position of strongest band or bands in a "complex" of features. [f] Major feature in the CH stretching region.

TABLE 6: Infrared Frequencies (cm^{-1}) and Intensities for Neutral Chrysene

experiment		theory[a]			
frequency in Ar (cm^{-1})	relative intensity[b]	irreducible representation	frequency (cm^{-1})	intensity (km/mol)	relative intensity[c]
d		a_u	233.0†	4.3	0.04
d		a_u	431.0	8.0	0.08
d		b_u	480.2	8.5	0.09
534.8	0.04	b_u	538.4†	2.1	0.02
552.9	0.03	a_u	554.4†	2.2	0.02
578.9	0.02	a_u	579.6	5.1	0.05
682.4[e]	0.11	b_u	685.2	11.0	0.11
761.0[e]	1.00	a_u	762.6	96.6	1.00
812.6	0.49	a_u	817.0	65.3	0.68
852.7, 854.7	0.01	b_u	849.6†	2.2	0.02
861.8	0.08	a_u	863.7	9.3	0.10
880.1	0.03	b_u	876.9†	3.6	0.04
945.9, 947.0	0.02	a_u	946.9†	4.0	0.04
1035.8[e]	0.07	b_u	1032.0	6.9	0.07
1162.8	0.004	b_u	1171.3†	2.8	0.03
1193.4[e]	0.04	b_u	1196.0†	2.3	0.02
1235.9[e]	0.04	b_u	1239.7†	2.9	0.03
1264.0	0.09	bu	1263.4	15.9	0.16
1270.6[e]	0.02				
1302.3	0.02				
1371.1	vw	b_u	1347.7†	2.6	0.03
1429.7 } 1437.1 }	0.16	b_u	1426.1	10.3	0.11
		b_u	1434.3†	4.8	0.05
1490.6	0.11	b_u	1484.7	8.7	0.09
1523.2	0.01	b_u	1514.6	9.4	0.10
1601.2, 1603.2[e]	0.06	b_u	1589.1	8.2	0.08
		b_u	1607.0	2.0	0.02
1946.1[e]	0.04				
3021.9					
3033.4					
3054.1		b_u	3048.9	20.2	0.21
3063.9[f]		b_u	3057.1	44.8	0.46
3079.4[f]		b_u	3073.8	84.0	0.87
3093.8		b_u	3084.8	17.3	0.18
3106.8		b_u	3101.1	68.7	0.71
3134.9					
Σ 3144-2997	1.12				
sum =				235.0	2.43

[a] Taken from ref 1. † indicates theoretical band not reported in original publication. [b] Intensities relative to the strongest observed band at 761.0 cm^{-1}. [c] Theoretical intensities given relative to the strength of the calculated 762.6 cm^{-1} band. [d] Theoretical position lying below the low-frequency limit of experimental data. [e] Position of strongest band of bands in a "complex" of features. [f] Major feature in the CH stretching region.

and theory is excellent for such a large molecule. The average difference in the frequencies of predicted and observed bands is 5 cm^{-1} and all differences are less than 13 cm^{-1}. Relative band strengths compare favorably, although not quite as well as in most of the other PAHs studied where agreements better than 50% were typical. The relative strengths of all the bands agree with theory to within factors of about 2.

The positions and strengths of the various bands of pyrene can also be compared with the previous matrix isolation[30] and gas-phase[15] studies (see Table 9 in ref 1). As was the case for naphthalene and anthracene, while the present work extends to greater sensitivity than previous matrix studies, for those bands that have been reported previously, there is excellent agreement between the data sets. The experimental band position agreements between the two matrix isolation studies are excellent with positions matching to within the accuracy of the data (1 cm^{-1}). These values are also in good agreement with the band positions reported for gas-phase pyrene at 300 °C.[15] Where reported (gas-phase values are not mentioned for many of the weaker bands), the gas-phase positions fall from about 1 to 7 cm^{-1} to the red of the matrix isolation values, again consistent

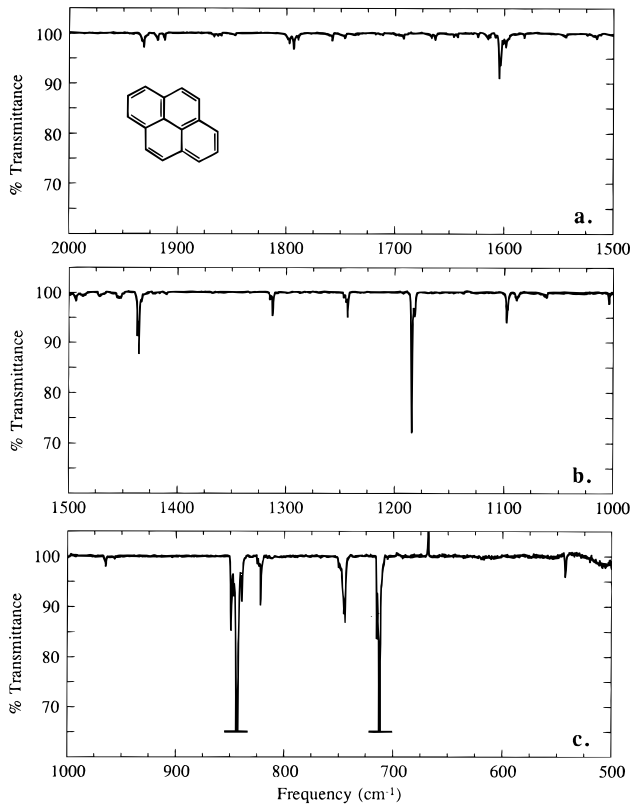

Figure 6. The spectra of matrix isolated pyrene ($C_{16}H_{10}$) through the aromatic CC stretching and CH bending regions: (a) 2000−1500 cm^{-1}, (b) 1500−1000 cm^{-1}, and (c) 1000−500 cm^{-1}. Several of the strongest CH out-of-plane bending mode bands have been truncated to enhance visibility of features across the spectrum. The sample was deposited and measured at 10 K and the argon-to-pyrene ratio was in excess of 1000/1.

with the finding that the infrared bands of PAHs are red-shifted as the temperature increases.[16]

The comparison of band strengths is more complicated, but in most cases there is satisfactory agreement between the theory and the various experimental data sets. There are, however, a number of bands where the agreement is marginal. Both matrix studies and the gas-phase study suggest that the predicted strength of the theoretical band at 710.9 cm^{-1} is approximately 1.5 times too weak (theory, 0.27; experiment, 0.43). The experimental data sets also suggest that the strength of the predicted band at 746.6 cm^{-1} is underestimated by a factor of 2 (theory, 0.08; experiment, 0.17). The two matrix studies suggest a similar underestimate for the predicted band at 1188.3 cm^{-1} (theory, 0.09; experiment, 0.19), although the reported gas-phase value for this band is similar to theory. Despite the uncertainty introduced by H_2O contamination, both matrix isolation studies suggest that the strength of the theoretical band at 1586.1 cm^{-1} is considerably too high (theory, 0.11; experiment, 0.005), although they disagree to what extent (no corresponding gas-phase band was reported). Furthermore, all three data sets agree that the intensity of the predicted band at 1597.0 cm^{-1} is about 1.8 times too low (theory, 0.05; experiment, 0.08).

6. 1,2-Benzanthracene, $C_{18}H_{12}$. The 2000−500 cm^{-1} spectrum of matrix isolated 1,2-benzanthracene is presented in Figure 7. The positions and strengths of the absorption bands are listed and compared to theoretical predictions[1] in Table 5. The relative strengths of the bands were normalized to the 747.0 cm^{-1} feature in the experimental data and to the predicted band at 748.9 cm^{-1}. Also, the symmetry species of the predicted bands at 3055.8 and 656.0 cm^{-1} were incorrectly given as a″ in ref 1 and have been changed to the correct a′ in Table 5.

TABLE 7: Infrared Frequencies (cm^{-1}) and Intensities for Neutral Tetracene

experiment		theory[a]			
frequency in Ar (cm^{-1})	relative intensity[b]	irreducible representation	frequency (cm^{-1})	intensity (km/mol)	relative intensity[c]
d		b_{1u}	160.7†	1.1	0.01
d		b_{3u}	465.1	22.3	0.27
d		b_{3u}	473.5†	1.1	0.01
551.6	0.11	b_{2u}	555.7	8.7	0.10
607.7	0.02	b_{1u}	610.9	1.8	0.02
627.7	0.01	b_{2u}	640.2†	1.4	0.02
		b_{2u}	735.4	2.1	0.03
742.9[e]	1.00	b_{3u}	747.2	84.7	1.00
766.7	0.01				
895.3[e]	0.84	b_{3u}	906.3	81.1	0.96
933.4	0.02	b_{1u}	935.6	1.9	0.02
953.6	0.08	b_{3u}	961.6	10.4	0.13
997.1	0.07	b_{2u}	995.8	3.6	0.04
1054.3	0.01				
1124.4, 1128.7	0.06	b_{1u}	1123.5	4.7	0.06
1165.3	0.02	b_{2u}	1145.2	3.6	0.04
1199.3	0.01	b_{1u}	1207.0†	2.0	0.02
1288.5[e]	0.02	b_{1u}	1283.0	11.5	0.14
1292.3	0.04	b_{1u}	1292.7	5.0	0.06
1298.8	0.08	b_{2u}	1292.8	0.8	0.01
1322.9[f]	0.02				
1337.9	0.05	b_{2u}	1337.8	8.2	0.10
1388.7	0.04	b_{1u}	1399.2	1.6	0.02
1416.1	0.02				
1465.2	0.04	b_{2u}	1469.6	3.9	0.04
1474.1	0.01				
1540.1	0.01	b_{2u}	1536.1	2.8	0.03
1546.2	0.02				
1554[e]	0.02	b_{1u}	1562.5	1.1	0.01
1573.2	0.03				
1637.0, 1640.7[g]	0.04	b_{1u}	1626.2	9.4	0.11
1685.5[e,f]	0.04				
1712.7[e]	0.05				
1730.9	0.01				
1786.0[e]	0.08				
1800.3[e]	0.03				
1819.8	0.01				
1836.3	0.01				
1904.2[e]	0.02				
1917.1[e]	0.02				
1933.3[e]	0.05				
2908.9					
2934.3					
2961.0					
3007.5					
3022.1					
3032.6					
3036.2		b_{2u}	3040.5†	1.9	0.02
		b_{1u}	3041.6	16.0	0.18
		b_{1u}	3044.5	32.9	0.38
		b_{2u}	3048.1†	1.4	0.02
3055.0[h]		b_{1u}	3063.7	81.2	0.96
3076.1		b_{2u}	3078.4	120.1	1.41
3090.3					
3095.5					
Σ 3106-2997 sum =	1.25			253.5	2.97

[a] Taken from ref 1. † indicates theoretical band not reported in original publication. [b] Intensities relative to the total observed absorbance produced by the band complex dominated by the 742.9 cm^{-1} feature. [c] Theoretical intensities given relative to the strength of the calculated 747.2 cm^{-1} band. Relative values are a factor of 1.41 larger than those in original publication.[1] [d] Theoretical position lying below the low-frequency limit of experimental data. [e] Position of strongest band in a "complex" of features. [f] Band possibly associated with 5,12-naphthacenequinone contaminant. [g] Band intensity uncertain due to overlap with bands produced by small amounts of contaminant H_2O. [h] Major feature in the CH stretching region.

TABLE 8: Infrared Frequencies (cm^{-1}) and Intensities for Neutral Triphenylene

experiment		theory[a]			
frequency in Ar (cm^{-1})	relative intensity[b]	irreducible representation	frequency (cm^{-1})	intensity (km/mol)	relative intensity[c]
d		a_2''	119.6†	2.1	0.01
d		a_2''	424.9†	4.1	0.02
619.8	0.06	e′	631.3	10.3	0.06
740.8[e]	1.00	a_2''	743.6	180.9	1.00
947.0	0.01	a_2''	947.2†	2.0	0.01
993.1	0.01	e′	996.3†	3.4	0.02
1054.2	0.02	e′	1054.6	6.9	0.04
1246.0, 1255.9[e]	0.06	e′	1253.8	6.5	0.04
1299.5	vw	e′	1292.5†	3.6	0.02
1437.7[e]	0.24	e′	1440.4	46.9	0.26
1501.1	0.10	e′	1498.2	25.3	0.14
1607.8	0.03	e′	1596.0†	0.9	0.01
1943.5[e]	0.02				
3038.8					
3049.4		e′	3054.1	5.3	0.03
3074.7		e′	3068.3	104.1	0.58
3090.9[f]		e′	3089.4†	2.4	0.01
3098.0[f]		e′	3105.3	123.3	0.68
3116.9					
Σ 3147-3023	0.53				
sum =				235.1	1.30

[a] Taken from ref 1. † indicates theoretical band not reported in original publication. [b] Intensities relative to the total observed absorbance produced by the band complex dominated by the 740.8 cm^{-1} band. [c] Theoretical intensities given relative to the strength of the calculated 743.6 cm^{-1} band. [d] Theoretical position lying below the low-frequency limit of experimental data. [e] Position of strongest band in a "complex" of features. [f] Major feature in the CH stretching region.

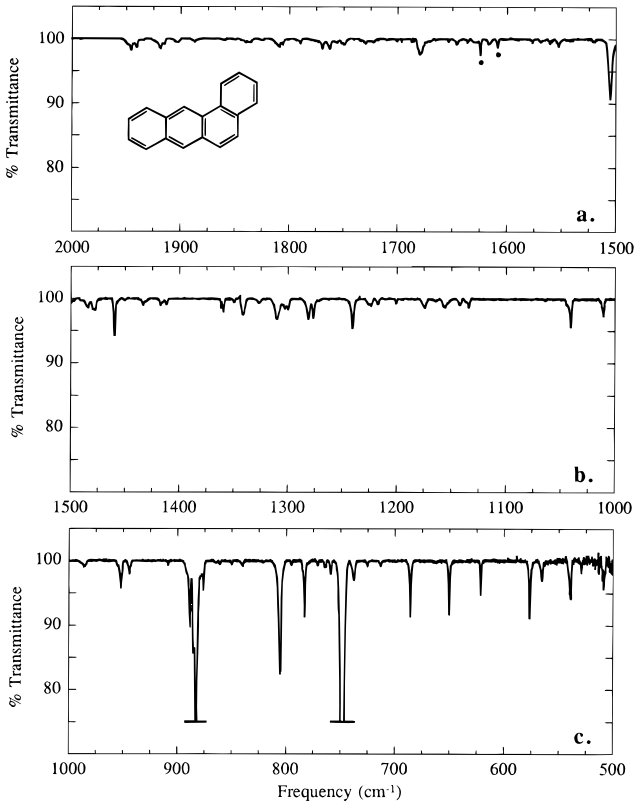

Figure 7. The spectra of matrix isolated 1,2-benzanthracene ($C_{18}H_{12}$) through the aromatic CC stretching and CH bending regions: (a) 2000−1500 cm^{-1}, (b) 1500−1000 cm^{-1}, and (c) 1000−500 cm^{-1}. Several of the strongest CH out-of-plane bending mode bands have been truncated to enhance visibility of features across the spectrum. The sample was deposited and measured at 10 K and the argon to 1,2-benzanthracene ratio was in excess of 1000/1.

Because of its lower symmetry (C_s), this molecule exhibits a particularly rich spectrum. As with the previous PAHs, the agreement between experiment and theory is generally quite good with the average difference in the frequencies of predicted and observed bands being 4 cm^{-1} and all differences less than 11 cm^{-1}. Agreement between the measured and calculated relative band strengths is comparable to that seen for pyrene. The relative strengths of the stronger bands all agree to within 35%. Moderate strength bands typically agree to within about 40%, although there are a few exceptional cases with considerably larger differences (see below). Weaker bands agree to better than a factor of 2.

Several bands are worthy of additional comment. First, theory predicts a moderately strong feature near 779.2 cm^{-1}. A band is observed near this position (782.5 cm^{-1}), but it is more than 2 times weaker than predicted (theory, 0.16; experiment, 0.07). A more dramatic mismatch involves the moderate theoretical band at 903.6 cm^{-1}. While this feature is observed at 908.4 cm^{-1}, its measured strength is more than an order of magnitude less than predicted (theory, 0.10; experiment, 0.003). The reason for such a striking discrepancy is not clear.

7. Chrysene, $C_{18}H_{12}$. The 2000−500 cm^{-1} spectrum of matrix isolated chrysene is presented in Figure 8. The positions and strengths of the absorption bands are listed and compared to theoretical predictions[1] in Table 6. The relative strengths of the bands were normalized to the sum of the band complex dominated by the 761.0 cm^{-1} feature in the experimental data and to the predicted band at 762.6 cm^{-1}.

Again, the agreement between experiment and theory is excellent. The average difference in the frequencies of predicted and observed bands is 4 cm^{-1} with all differences less than about 12 cm^{-1}. Relative band strengths also compare favorably. The relative strengths of the stronger bands agree to within 30%. Moderately strong bands typically agree to better than 20%, although there are several notable exceptions (see below). Weaker bands generally agree to better than a factor of 2−3.

Several of the bands of moderate strength require additional discussion. A number of the absorption features in the spectrum of the matrix isolated chrysene appear in band "complexes" that consist of a main feature associated with a secondary feature falling about 7 cm^{-1} higher in frequency and with about one-fourth the intensity. This pattern is likely due to site effects in the matrix with both bands arising from the same vibrational mode. In view of this, it is possible that the experimentally observed features at 1264.0 and 1270.6 cm^{-1} are both associated with the single predicted mode at 1263.4 cm^{-1}. Even so, the predicted strength of this band (0.16) would still exceed the combined strength of the 1264.0/1270.6 cm^{-1} complex (0.11) by close to 30%. The same site effects may be responsible for the complicated overlap of features in the 1440−1430 cm^{-1} region. The experimental bands at 1429.7 and 1437.1 cm^{-1} provide good frequency matches to the theoretical bands at 1426.1 and 1434.3 cm^{-1}, respectively, but the bands (and their satellites) overlap enough that their individual strengths cannot be measured. However, the combined strengths of the two experimental and theoretical bands (both 0.16) agree well and it is apparent from the spectrum in Figure 8 that the relative strengths of the bands are at least qualitatively consistent with the predictions (1426.1 cm^{-1}, 0.11; 1434.3 cm^{-1}, 0.05).

The largest discrepancy between the experimental and theoretical results is for the band predicted at 1514.6 cm^{-1} and observed at 1523.2 cm^{-1}. According to the calculations, this band should have a relative strength of 0.10, but experimentally the band is observed to be 10 times weaker. Again, the source

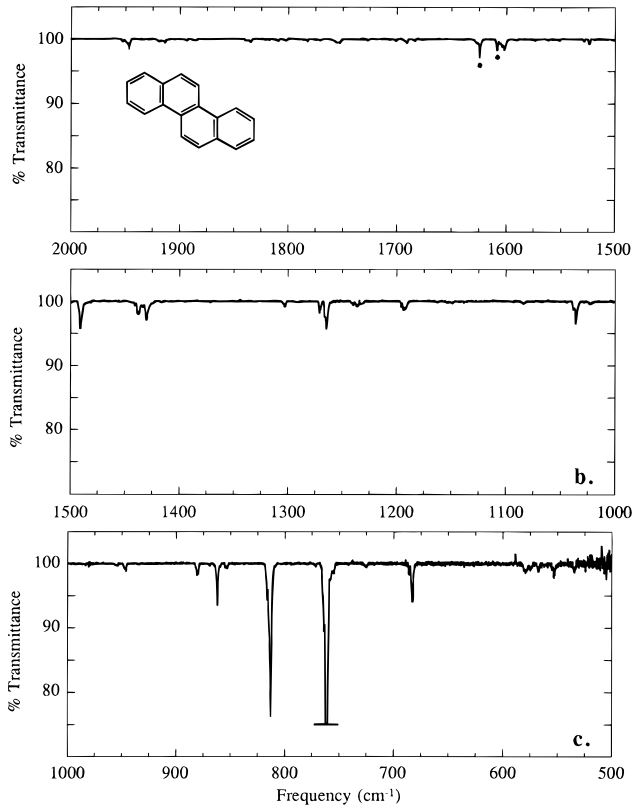

Figure 8. The spectra of matrix isolated chrysene ($C_{18}H_{12}$) through the aromatic CC stretching and CH bending regions: (a) 2000−1500 cm^{-1}, (b) 1500−1000 cm^{-1}, and (c) 1000−500 cm^{-1}. The strongest CH out-of-plane bending mode band has been truncated to enhance visibility of features across the spectrum. The sample was deposited and measured at 10 K and the argon-to-chrysene ratio was in excess of 1000/1.

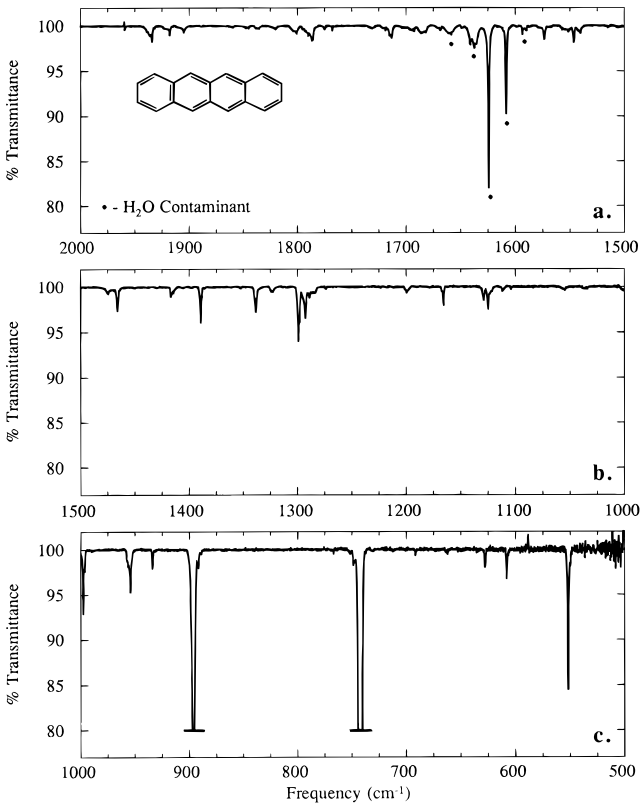

Figure 9. The spectra of matrix isolated tetracene ($C_{18}H_{12}$) through the aromatic CC stretching and CH bending regions: (a) 2000−1500 cm^{-1}, (b) 1500−1000 cm^{-1}, and (c) 1000−500 cm^{-1}. Several of the strongest CH out-of-plane bending mode bands have been truncated to enhance visibility of features across the spectrum. The sample was deposited and measured at 10 K and the argon-to-tetracene ratio was in excess of 1000/1.

of this difference is not clear. The predicted band at 1171.3 cm^{-1}, although weak (0.03), shows a similarly large departure from its experimental counterpart at 1162.8 cm^{-1} (0.004).

Finally, the absorption complex dominated by the bands at 1603.2 and 1601.2 cm^{-1} probably corresponds to the theoretical 1607.0 and 1589.1 cm^{-1} features, although the strengths of the experimental bands could not be measured individually. Nevertheless, the relative depths of the two components in the complex (see Figure 8) are qualitatively similar to that predicted (1607.0 cm^{-1}, 0.02; 1589.1 cm^{-1}, 0.08) and the measured intensity of the complex (0.06) is not inconsistent with the sum of the theoretical intensities given the uncertainty associated with H_2O contamination in this region.

8. Tetracene, $C_{18}H_{12}$. The 2000−500 cm^{-1} spectrum of matrix isolated tetracene is presented in Figure 9. The positions and strengths of the absorption bands are listed and compared to theoretical predictions[1] in Table 7. The relative strengths of the experimental bands were normalized to the sum of the band complex dominated by the 742.9 cm^{-1} feature. The theoretical relative band strengths, which were normalized to the theoretical 3078.4 cm^{-1} CH stretching band in the original publication, have been renormalized to the strongest predicted aromatic CH out-of-plane bending feature at 747.2 cm^{-1}. Thus, the theoretical relative strengths reported in Table 7 have been scaled by a factor of 1.41 relative to those in Table 4 of ref 1.

The agreement between the experimental matrix isolation results and theory, while generally very good, is perhaps not quite as good as for many of the other PAHs studied, making it occasionally difficult to uniquely assign the band correspondences. The average difference in the frequencies of predicted and observed bands is about 7 cm^{-1}. With the exception of a few weak features where the band correspondences are open to question, all the frequency differences are less than 13 cm^{-1}. The relative strengths of the stronger bands in the 2000−500 cm^{-1} range agree to within 15%. Moderately strong bands typically agree to better than 50%, although there are several exceptions (see below). Weaker bands agree to better than a factor of 2 with one exception (see below).

In addition to the available theoretical calculations, the positions and strengths of the various bands of tetracene can also be compared to previously published matrix isolation studies[29] (see Table 4 in ref 1). Again, although the work reported here extends to weaker features than the earlier matrix studies, where comparisons are possible, the band position agreements are excellent. Interestingly, there are a number of anomalous bands reported in the earlier studies that *do not* appear to arise from tetracene, most notably the bands at 1397.1/1398.6, 1321.4, and 964.7 cm^{-1}. These differences (as well as several band strength discrepancies with theory outlined below) are probably related to a contaminant in the tetracene sample. During the course of the studies reported here, it was observed that the spectra of different tetracene samples often contained a family of bands that varied in strength independently of the primary tetracene bands. This family of bands contained members at 576.9(w), 711.8(w), 751.4(w), 923.5(vw), 965.0(m), 1162(w), 1210.6(w), 1225.4(vw), 1283.7(s), 1321.0(m), 1351.7(w), 1360.3(w), 1377.1(vw), 1398.9(m), 1460.5(m), and 1685.7(m) cm^{-1}. The most likely tetracene contaminant is the synthetic

precursor 5,12-naphthacenequinone (Aldrich Chemical Co., private communication). Examination of the spectrum of 5,12-naphthacenequinone[37] confirmed that indeed the majority of these features are attributable to this compound. Since the bands reported in the earlier matrix studies are among the strongest in the spectrum of 5,12-naphthacenequinone, and since the tetracene used in those studies was obtained from the same source, it is likely that the bands in question are due to this contaminant. The 5,12-naphthacenequinone contaminant was largely removed by baking the sample under dynamic vacuum for several hours prior to deposition.

The comparison of band strengths, while complicated by the aforementioned contaminant, still shows generally good agreement between the theory and the experimental data sets. There are, however, a number of bands that require specific comment. There is no experimental evidence for the weak predicted band at 735.4 cm^{-1}. However, this band may fall within the envelope of the very strong band observed at 742.9 cm^{-1}. The very weak band observed at 766.7 cm^{-1} does not correspond to any expected infrared-active vibration. However, it does correspond to an infrared *inactive* b_{2g} vibrational mode that is predicted to fall at 763.2 cm^{-1} (Langhoff, private communication). It is possible that this vibrational mode is weakly activated by matrix interactions. The observed band at 953.6 cm^{-1} is about 40% weaker than the corresponding predicted band at 961.6 cm^{-1} (theory, 0.13; experiment, 0.08), but is consistent with the value reported in the previous matrix isolation studies.[29] Furthermore, both matrix experiments report two bands (1124.4 and 1128.7 cm^{-1}) which may corresponding to the predicted band at 1123.5 cm^{-1}. These likely represent site splitting of the same vibrational mode, and their combined strengths agree well with that predicted.

The moderately weak band predicted at 1145.2 cm^{-1} is problematic. Neither the experiments reported here nor the previous matrix studies[29] exhibit a band near this position. However, both matrix studies show a band of appropriate strength at about 1165.3 cm^{-1}, requiring an unusually large discrepancy with the calculated position. While the 1165.3 cm^{-1} position falls near a very weak feature of 5,12-naphthacenequinone, simple band scaling suggest that the contaminant is probably not responsible. In any event, the weak predicted 1145.2 cm^{-1} band implies a larger than average mismatch with experiment in either position or strength.

The three bands predicted at 1283.0, 1292.7, and 1292.8 cm^{-1} (predicted relative intensities 0.14, 0.06, and 0.01, respectively) are also somewhat problematic. The three corresponding experimental bands likely fall at 1288.5, 1292.3, and 1298.8 cm^{-1} (relative intensities 0.02, 0.04, and 0.08, respectively). Given the available data it is not possible to positively identify the corresponding band pairs, but it is clear by comparing the sums of the measured and predicted strengths (0.14 and 0.21, respectively) that there is a significant discrepancy between the two. The correspondences given in Table 7 are simply those which give the best *positional* agreement between experiment and theory. On the other hand, based purely on the *individual strengths* of the bands, it is tempting to suggest the correspondences (theory ↔ experiment): 1283.0 ↔ 1298.8 cm^{-1}, 1292.7 ↔ 1292.3 cm^{-1}, and 1292.8 ↔ 1288.5 cm^{-1}. Although this implies a somewhat larger than normal discrepancy in frequency for the 1283.0/1298.8 cm^{-1} band pair, such an assignment would indicate that the majority of the mismatch is associated only with this pair and that the other two are in good agreement. Nevertheless, the agreement between experimental and theoretical positions has consistently exceeded that for the relative strengths, and given the possibility that a resonance between these closely spaced modes could be modifying their relative intensities, the correspondences in Table 7 are perhaps the most conservative. The previous matrix study reported bands at 1284.3, 1292.5, and 1298.8 cm^{-1}, the latter two of which agree well in both position and strength with those reported here. The reported 1284.3 cm^{-1} band does provide a better match in both position and intensity to the predicted 1283.0 cm^{-1} feature, but in all likelihood arises from the contaminant 5,12-naphthacenequinone whose strongest band falls precisely at this position. The strength they report for the band is consistent with that expected if the other features they list at 964.7, 1165.2, 1321.4, and 1398.6/1397.1 cm^{-1} are also due to 5,12-naphthacenequinone. Both sets of matrix isolation studies agree that the predicted bands at 1337.8 and 1626.2 cm^{-1}: have strengths that are 2.0 to 2.5 too large (theory/experiment, 1337.8 cm^{-1}: 0.10/0.05. 1626.2 cm^{-1}: 0.11/0.04), although the latter deviation may merely reflect the uncertainty introduced by contaminant H_2O in this region of the spectrum.

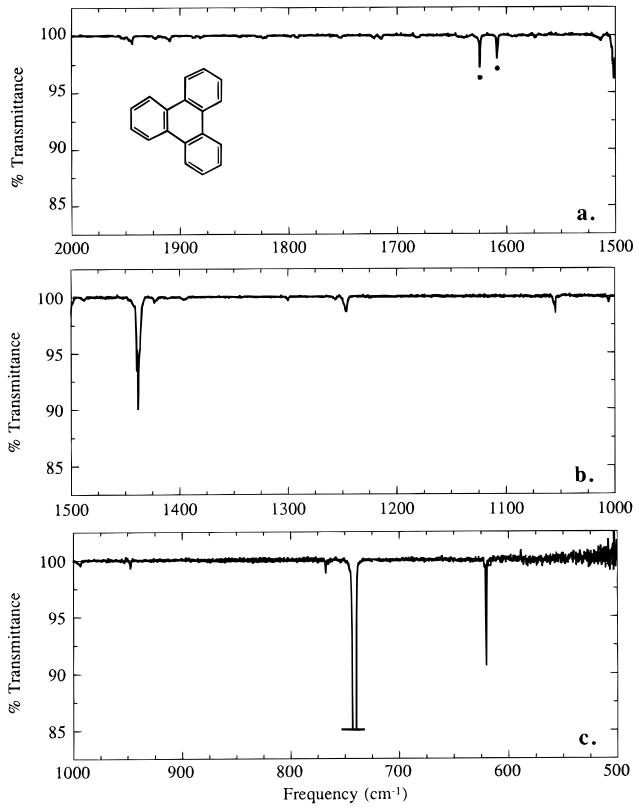

Figure 10. The spectra of matrix isolated triphenylene ($C_{18}H_{12}$) through the aromatic CC stretching and CH bending regions: (a) 2000−1500 cm^{-1}, (b) 1500−1000 cm^{-1}, and (c) 1000−500 cm^{-1}. The strongest CH out-of-plane bending mode band has been truncated to enhance visibility of features across the spectrum. The sample was deposited and measured at 10 K and the argon-to-triphenylene ratio was in excess of 1000/1.

9. Triphenylene, $C_{18}H_{12}$. The 2000−500 cm^{-1} spectrum of matrix isolated triphenylene is presented in Figure 10. The positions and strengths of the absorption bands are listed together with their theoretically predicted values[1] in Table 8. The relative strengths of the bands were normalized to the 740.8 cm^{-1} feature in the experimental data and to the predicted band at 743.6 cm^{-1}. Because of its high degree of symmetry (D_{3h}), this molecule exhibits a relatively simple spectrum. It should be noted that in the original theoretical paper[1] the symmetry species of the

modes corresponded to D_{2h} symmetry and that these have been corrected to reflect the full D_{3h} symmetry of the molecule in Table 8.

Again, the agreement between experiment and theory is generally very good. The average difference in the frequencies of predicted and observed bands is 5 cm^{-1} and all the frequency differences are less than 12 cm^{-1}. The relative strengths of the strong and moderately strong bands all agree to within 25%, most to better than 10%. Weaker bands all agree to within a factor of 2 to 3. In view of the relative simplicity of the spectrum and the overall good agreement with the theory, no further discussion is warranted for this molecule.

C. Implications for Astrophysics. The spectra presented in the previous section and in the companion articles which appear subsequently in this journal issue[31,32] can be used to examine the extent to which neutral PAHs contribute to the interstellar infrared emission features. The original suggestions that this family of emission features was due to PAHs were founded on the general resemblance of the interstellar emission spectra to the then-available laboratory absorption spectra of aromatic hydrocarbons. One of the early objections to the PAH hypothesis was that, while the *positions* of the interstellar and laboratory PAH bands were similar, their *relative strengths* were not. In particular, the family of interstellar bands is dominated by the features at 1610, 1310, and 1160 cm^{-1}, which are attributed to various CC modes and CH in-plane bending modes. The 3050 cm^{-1} band, assigned to CH stretching modes, and the 885, 840, and 787 cm^{-1} bands, assigned to out-of-plane CH bending modes, are generally considerably weaker. In contrast, the relative strengths of these various bands are observed in the laboratory to be reversed in the spectra of neutral PAHs. However, the early laboratory spectra were taken from PAHs in solvents, in salt pellets, or in pure form, while the PAHs in interstellar space are thought to be largely in the gas phase.[6] Since it was known that PAH−PAH interactions in solid samples can strongly alter the frequencies and intensities of their vibrational modes, especially the CH out-of-plane banding modes,[7] it was not clear whether the mismatch represented a fundamental failure of the PAH hypothesis. The laboratory spectra of matrix isolated and gas-phase PAHs can be used to address this issue.

Comparison of the matrix isolation data on PAH neutrals with the spectra of PAH samples in KBr demonstrates that matrix isolated PAHs do, in fact, produce significantly weaker CH out-of-plane bending mode bands. However, the decrease in the strength of these bands relative to the higher frequency modes is *not* sufficiently large to bring the PAH spectra in line with typical interstellar emission spectra. Figure 11 shows a comparison of the infrared spectrum of the planetary nebula BD+30°3639, which produces a fairly characteristic interstellar emission band family, with a schematic "stick spectrum" of a mixture of the neutral PAHs presented here and in the companion papers.

It is immediately apparent from Figure 11 that, while mixtures of neutral PAHs do produce features that fall near the characteristic frequencies seen in the interstellar spectrum, they still do not provide a good fit to the relative band strengths. Thus, the spectra of matrix isolated neutral PAHs represent a *quantitative* improvement to the interstellar match, but not a *qualitative* one. Instead, it appears that a far better fit is provided by PAH cations (Figure 11c). For cations, the relative band strengths between the lower and higher frequency modes are reversed. The result is a much better match to the interstellar

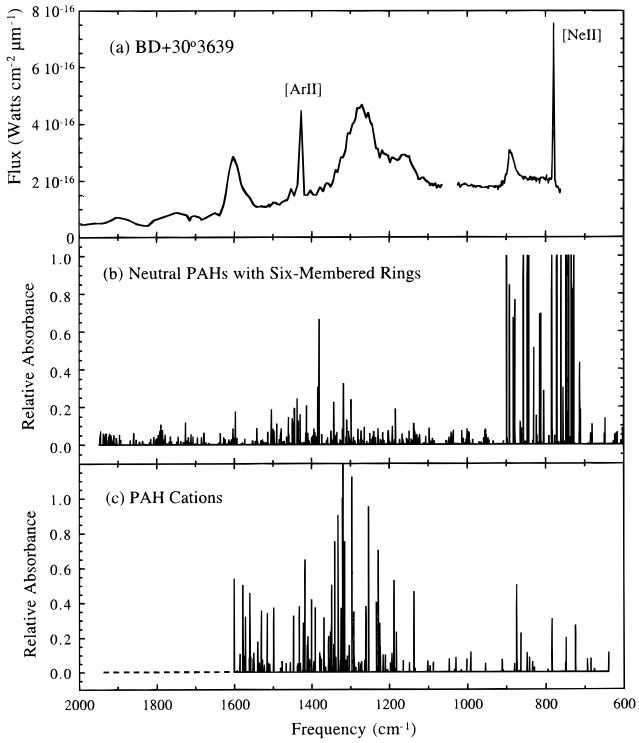

Figure 11. The 2000−600 cm^{-1} spectra of (a) the planetary nebula BD+30°3639, (b) a mixture of neutral PAHs, and (c) a mixture of PAH cations. The sharp emission features near 1440 and 780 cm^{-1} in the spectrum of BD+30°3639 are due to singly ionized atomic Ar and singly ionized atomic Ne, respectively. The remaining features are thought to be due to a mixture of PAHs. The astronomical data is a composite based on data from refs 7, 38, and 41. The mixture of neutral PAHs includes all the species reported in this paper and in ref 31. The composite PAH ion spectrum was made using data taken from refs 22−25 and unpublished data, and it includes the features of ionized naphthalene, phenanthrene, pyrene, benzo[*e*]pyrene, benzo[ghi]perylene, coronene, and benzo[*k*]fluoranthene.

spectrum. Detailed discussions of the infrared spectra of PAH cations and their infrared spectra can be found elsewhere.[1,23−30]

Domination of the typical interstellar emission spectra by PAH cations is not unexpected. The interstellar emission spectrum originates in environments with large UV radiation fluxes. It is the absorption of this UV that excites the PAHs and causes them to fluoresce in the infrared. This same UV is also expected to ionize the PAHs. In regions where the UV flux is lower, such as in the envelopes of carbon stars and in protoplanetary nebulae, neutral PAHs may well dominate the PAH population. However, environments that contain less UV, and therefore more PAH neutrals, also produce less fluorescent emission. Thus, the astronomical data contain a significant selection effect in favor of the detection of environments dominated by PAH cations. There are, however, a few carbon-rich objects that produce emission spectra that can be better fit if significant contributions from PAH neutrals are included with those of the ions. These objects have more benign UV radiation fields, a point qualitatively consistent with an expected increased contribution from neutral PAHs.

With regards to astrophysical implications, one final characteristic of the data is worthy of special note. Allamandola et al.[38] have shown that the interstellar emission band family includes weak features near 1750 and 1920 cm^{-1} (5.7 and 5.2 μm). These features would not have been predicted on the basis of a theoretical consideration of the fundamental modes of PAHs. However, *all* the PAHs studied in the laboratory exhibit weak features in this spectral region. These features arise from

overtone/combination modes of lower frequency fundamentals and should be observed regardless of ionization state.

The full application of our database of PAH spectra to the astrophysical problem will be presented in refs 39 and 40.

IV. Conclusions

The infrared absorption spectra of eight different argon-matrix-isolated PAHs have been measured. The PAHs ranged in size from two to four rings. The resulting band positions and relative strengths were compared to previous laboratory studies, where available, and with available theoretical calculations.[1] Agreement with this previous work is excellent.

Comparisons with the theoretical data indicate that the density functional theory (DFT) does an excellent job of describing the majority of the infrared active fundamentals of the PAHs considered here. Band position matches generally agree very well, typically to within 5 cm^{-1}. The worst mismatches are almost always less than 15 cm^{-1}, and the few cases that exceed this are always weak bands where band correspondences between experiment and theory may be in question or where matrix effects are important.

Matches in band strengths are not as precise as matches in frequencies, but are generally good to better than 35% for most strong and medium bands and are good to factors of 2 to 3 for weaker bands. The larger difference for the weak bands may be partially due to the increased importance of matrix effects. Despite the generally good match between experiment and theory, individual PAH spectra can contain a small number of medium-to-strong bands that show significant differences (factors of 2) between experiment and theory. While these discrepancies can fall within the entire frequency range, the largest number lie in the 1600−1100 cm^{-1} region which is dominated by CC stretching and CH in-plane bending modes and represents the richest region of the spectra. The most likely explanation for most of the larger mismatches is that the theory fails to completely represent the degree of mixing between similar modes that fall close in frequency. The predicted extent of mixing is very sensitive to the level of calculation and minor mismatches in band positions can result in substantial mismatches in intensity.

The most consistent and dramatic difference between the experimental and theoretical results is in the CH stretching region. Theory consistently predicts band intensities that are too strong by about a factor of 2. These mismatches in intensity are supported by other available matrix isolation and gas-phase studies of PAHs. Some of this discrepancy may be due to matrix effects, but most of it is due to limitations in the theoretical treatment. The B3LYP/4-31G calculations probably overestimate the CH stretch by about a factor of 2 due to the relatively small 4-31G basis set used for the calculations.

The experimental spectra contain large numbers of bands not predicted by theory. Most (but not all) of these features are weak and are likely due to overtone/combination modes which are not addressed in the calculations. While these modes have not been addressed in any detail here, their absorption bands can be appreciable and could play an important role in PAH identification.

Finally, comparisons between the infrared spectra of matrix isolated neutral PAHs and the interstellar emission band family characteristic of environments having high UV fields indicate that neutral PAHs do not provide an overall good fit to the vast majority of the astronomical data. Neutral PAHs produce features at appropriate frequencies, but these features have inappropriate relative strengths. However, significant contributions from PAH neutrals may be required to explain the spectra of a few carbon-rich astronomical objects that produce atypical emission spectra. These objects tend to have more benign UV radiation fields, a point qualitatively consistent with an increased contribution from neutral PAHs.

Acknowledgment. The authors would like to thank S. Langhoff and C. Bauschlicher for useful conversations and for providing unabridged versions of their computational results, L. Allamandola for advice and support during this research and R. Walker for expert technical assistance. This work was carried out under NASA Grants 344-02-06-01 (Astrophysics Program) and 459-60-61-01 (Long Term Space Astrophysics Program).

References and Notes

(1) Langhoff, S. R. *J. Phys. Chem.* **1996**, *100*, 2819.

(2) (a) Lee, M. L.; Novotny, M. V.; Bartle, K. D. *Analytical Chemistry of Polycyclic Aromatic Compounds*; Academic Press: New York, 1981; Chapter 2. (b) Yürüm, Y., Ed. *New Trends in Coal Science*; NATO ASI Series, Series C: Mathematical and Physical Sciences; Kluwer Academic Publishers: Dordrecht, 1988; Vol. 244.

(3) (a) Harris, S. J.; Weiner, A. M. *Combust. Sci. Technol.* **1983**, *31*, 155. (b) Frenklach, M.; Warnatz, J. *Combust. Sci. Technol.* **1987**, *51*, 265.

(4) Harvey, R. G., Ed. *Polycyclic Hydrocarbons and Carcinogenesis*; American Chemical Society: Washington, DC, 1985.

(5) (a) Duley, W. W.; Williams, D. A. *Mon. Not. R. Astron. Soc.* **1981**, *196*, 269. (b) Leger, A.; Puget, J. L. *Astron. Astrophys.* **1984**, *137*, L5. (c) Allamandola, L. J.; Tielens, A. G. G. M.; Barker, J. R. *Astrophys. J.* **1985**, *290*, L25.

(6) Allamandola, L. J.; Tielens, A. G. G. M.; Barker, J. R. *Astrophys. J., Suppl. Ser.* **1989**, *71*, 733.

(7) Witteborn, F. C.; Sandford, S. A.; Bregman, J. D.; Allamandola, L. J.; Cohen, M.; Wooden, D. *Astrophys. J.* **1989**, *341*, 270.

(8) Lippencott, E. R.; O′Reilly, E. J. *J. Chem. Phys.* **1955**, *23*, 238 and references therein.

(9) (a) Whitmer, J. C.; Cyvin, S. J.; Cyvin, B. N. *Z. Naturforsch.* **1978**, *33A*, 45. (b) Bakke, A.; Cyvin, B. N.; Whitmer, J. C.; Cyvin, S. J.; Gustavsen, J. E.; Klaeboe, P. *Z. Naturforsch.* **1979**, *34A*, 579. (c) Cyvin, S. J.; Cyvin, B. N.; Brunvoll, J.; Whitmer, J. C.; Klaeboe, P.; Gustavsen, J. E. *Z. Naturforsch.* **1979**, *34A*, 876. (d) Cyvin, S. J. *J. Mol. Struct.* **1982**, *79*, 423. (e) Cyvin, B. N.; Klaeboe, P.; Whitmer, J. C.; Cyvin, S. J. *Z. Naturforsch.* **1982**, *37A*, 251. (f) Cyvin, S. J.; Cyvin, B. N.; Brunvoll, J.; Whitmer, J. C.; Klaeboe, P. *Z. Naturforsch.* **1982**, *37A*, 1359. (g) Cyvin, B. N.; Cyvin, S. J. *Spectrosc. Lett.* **1986**, *19*, 1161.

(10) (a) Flickinger, G. C.; Wdowiak, T. J. *Astrophys. J.* **1990**, *362*, L71. (b) Colangeli, L.; Mennella, V.; Bussoletti, E. *Astrophys. J.* **1992**, *385*, 577. (c) Colangeli, L.; Mennella, V.; Baratta, G. A.; Bussoletti, E.; Strazzulla, G. *Astrophys. J.* **1992**, *396*, 369.

(11) Sellgren, K. *Astrophys. J.* **1984**, *277*, 623.

(12) (a) DeFrees, D. J.; Miller, M. D. In *Interstellar Dust: Contributed Papers*; Allamandola, L. J., Tielens, A. G. G. M., Eds.; NASA Conference Proceeding CP-3036, National Aeronautics and Space Administration: Washington, DC, 1989; p 173. (b) Pauzat, F.; Talbi, D.; Miller, M. D.; DeFrees, D. J.; Ellinger, Y. *J. Phys. Chem.* **1992**, *96*, 7882. (c) Rougeau, N.; Flament, J. P.; Youkharibache, P.; Gervais, H. P.; Berthier, G. *J. Mol. Struct. (THEOCHEM)* **1992**, *254*, 405. (d) Talbi, D.; Pauzat, F.; Ellinger, Y. *Astron. Astrophys.* **1993**, *268*, 805. (e) Cebe, E.; Grampp, G. *Z. Phys. Chem.* **1994**, *187*, 15.

(13) Bauschlicher, C. W., Jr.; Langhoff, S. R.; Sandford, S. A.; Hudgins, D. M. *J. Phys. Chem. A* **1997**, *101*, 2414.

(14) (a) Flickinger, G. C.; Wdowiak, T. J.; Gomez, P. L. *Astrophys. J.* **1991**, *380*, L43. (b) Semmler, J.; Yang, P. W.; Crawford, G. E. *Vib. Spectrosc.* **1991**, *2*, 189. (c) Kurtz, J. *Astron. Astrophys.* **1992**, *255*, L1.

(15) Joblin, C.; d'Hendecourt, L.; Léger, A.; Defourneau, D. *Astron. Astrophys.* **1994**, *281*, 923.

(16) Joblin, C.; Boissel, P.; Léger, A.; d'Hendecourt, L.; Defourneau, D. *Astron. Astrophys.* **1995**, *299*, 835.

(17) (a) Cherchneff, I.; Barker, J. R. *Astrophys. J.* **1989**, *341*, L21. (b) Shan, J.; Suto, M.; Lee, L. C. *Astrophys. J.* **1991**, *383*, 459. (c) Brenner, J.; Barker, J. *Astrophys. J.* **1992**, *388*, L39.

(18) Schlemmer, S.; Cook, D. J.; Harrison, J. A.; Wurfel, B.; Chapman, W.; Saykally, R. J. *Science* **1994**, *265*, 1686.

(19) Cook, D. J.; Schlemmer, S.; Balucani, N.; Wagner, D. R.; Steiner, B.; Saykally, R. J. *Nature* **1996**, *380*, 227.

(20) Hallam, H. E., Ed. *Vibrational Spectroscopy of Trapped Species*; John Wiley & Sons: New York, 1973.

(21) (a) Mamantov, G.; Wehry, E. L.; Kemmerer, R. R.; Hinton, E. R. *Anal. Chem.* **1977**, *49*, 86. (b) Wehry, E. L.; Mamantov, G.; Kemmerer, R. R.; Stroupe, R. C.; Tokousbalides, P. T.; Hinton, E. R.; Hembree, D. M.;

Dickinson, R. B., Jr.; Garrison, A. A.; Bilotta, P. V.; Gore, R. R.*Carcinogenesis* **1982**, *3*, 193. (c) Hembree, D. M.; Garrison, A. A.; Crocombe, R. A.; Yokley, R. A.; Wehry, E. L.; Mamantov, G. *Anal. Chem.* **1981**, *53*, 1783.

(22) Hudgins, D. M.; Sandford, S. A.; Allamandola, L. J. *J. Phys. Chem.* **1994**, *98*, 4243.

(23) Hudgins, D. M.; Allamandola, L. J. *J. Phys. Chem.* **1995**, *99*, 3033.

(24) Hudgins, D. M.; Allamandola, L. J. *J. Phys. Chem.* **1995**, *99*, 8978.

(25) Hudgins, D. M.; Allamandola, L. J. *J. Phys. Chem. A* **1997**, in press.

(26) Szczepanski, J.; Vala, M. *Astrophys. J.* **1993**, *414*, 646.

(27) (a) Szczepanski, J.; Roser, D.; Personette, W.; Eyring, M.; Pellow, R.; Vala, M. *J. Phys. Chem.* **1992**, *96*, 7876. (b) Szczepanski, J.; Chapo, C.; Vala, M. *Chem. Phys. Lett.* **1993**, *205*, 434. (c) Szczepanski, J.; Wehlburg, C.; Vala, M. *Chem. Phys. Lett.* **1995**, *232*, 221.

(28) Szczepanski, J.; Vala, M.; Talbi, D.; Parisel, O.; Ellinger, Y. *J. Chem. Phys.* **1993**, *98*, 4494.

(29) Szczepanski, J.; Drawdy, J.; Wehlburg, C.; Vala, M. *Chem. Phys. Lett.* **1995**, *245*, 539.

(30) Vala, M.; Szczepanski, J.; Pauzat, F.; Parisel, O.; Talbi, D.; Ellinger, Y. *J. Phys. Chem.* **1994**, *98*, 9187.

(31) Hudgins, D. M.; Sandford, S. A. *J. Phys. Chem. A* **1997**, 345.

(32) Hudgins, D. M.; Sandford, S. A. *J. Phys. Chem. A* **1997**, 356.

(33) Langhoff, S. R.; Bauschlicher, C. W., Jr.; Hudgins, D. M.; Sandford, S. A.; Allamandola, L. J. *J. Phys. Chem. A* **1997**, submitted for publication.

(34) Zhang, K.; Guo, B.; Colarusso, P.; Bernath, P. F. *Science* **1996**, *274*, 582.

(35) Joblin, C. Ph.D. Thesis, l'Université Paris 7, 1992.

(36) Bauschlicher, C. W., Jr.; Langhoff, S. R. *Spectrochim. Acta A*, **1997**, *53*, 1225.

(37) Pouchert, C. J. *The Aldrich Library of Infrared Spectra, 3rd ed.*; Aldrich Chemical Co., Inc: Milwaukee, Wisconsin, 1981; Spectrum 898C.

(38) Allamandola, L. J.; Bregman, J. D.; Sandford, S. A.; Tielens, A. G. G. M.; Witteborn, F. C.; Wooden, D. H.; Rank, D. *Astrophys. J.* **1989**, *345*, L59.

(39) Allamandola, L. J.; Hudgins, D. M.; Sandford, S. A. *Science* **1997**, submitted for publication.

(40) Hudgins, D. M.; Allamandola, L. J.; Sandford, S. A. *Astrophys. J.*, in preparation.

(41) Sandford, S. A. *Meteorit. Planet. Sci.* **1996**, *31*, 449.